Chapter 4
Relativistic Cyclotron

Abstract This Chapter is a brief introduction to the relativistic cyclotron accelerator, hands-on: by numerical simulation. It begins with a brief reminder of the historical context, and introduces the theoretical material needed for the simulation exercises. The Chapter relies on the basic charged particle optics and acceleration concepts introduced in Chapter 3, and further addresses

- Thomas focusing and the AVF cyclotron,
- positive focusing index,
- isochronous optics,
- separated sector cyclotrons,
- spin dynamics in an AVF cyclotron.

Simulations use optical elements met earlier: TOSCA, DIPOLE, CAVITE, SPNTRK, etc. They further develop on the modeling of sector dipoles, edge focusing and flutter, isochronous optics, separated sector ring cyclotrons, and simulation of these type of optics using DIPOLE, DIPOLES and CYCLOTRON keywords.

Notations used in the Text

B; B_0	field value; at reference radius R_0
$\mathbf{B}$; B_R; B_y	field vector; radial component; axial component
$B\rho = p/q$; $B\rho_0$	particle rigidity; reference rigidity
C; C_0	orbit length, $C = 2\pi R$; reference, $C_0 = 2\pi R_0$
E	particle energy
EFB	Effective Field Boundary
f_{rf}	RF frequency
h	RF harmonic number
$k = \frac{R}{B}\frac{dB}{dR}$	geometric index, a global quantity
$n = \frac{\rho}{B}\frac{dB}{d\rho}$	focusing index, a local quantity
m; m_0; M	mass; rest mass; in units of MeV/c^2
$\mathbf{p}$; p_0	particle momentum vector; reference momentum
q	particle charge
R	orbital radius
R_0; R_E	Reference radius at a reference energy; at energy E
s	path variable
v	particle velocity
V(t); $\hat{V}$	oscillating voltage; its peak value
x, x’, y, y’	radial and axial coordinates in moving frame
$\beta = v/c$; β_0; β_s	normalized particle velocity; reference; synchronous
$\gamma = E/m_0$	Lorentz relativistic factor
Δp, δp	momentum offset
ϵ_R	strength of a depolarizing resonance
ε_u	Courant-Snyder invariant (u: x, r, y, l, Y, Z, s, etc.)
ϕ; ϕ_s	particle phase at voltage gap; synchronous phase

Introduction

The loss of isochronism due to the relativistic increase of the mass limits the energy reach of the classical cyclotron. Vertical focusing in the latter imposes on the other hand slowly decreasing field with radius, *i.e.*, a negative index $-1 < k < 0$. Isochronism requires instead an increasing field with radius, field index $k > 0$, a consequence of $B(R) \propto \gamma(R)$, a property addressed below. The classical cyclotron technology eventually culminated with the construction at Berkeley in 1946 of a 184 in, 4000 ton cyclotron - soon turned into a synchrocyclotron, following the discovery of longitudinal phase stability.

Thomas azimuthally varying field (AVF) concept (Fig. 4.1), introduced in 1938[1] [3], allowed overcoming that conflict between vertical focusing and isochro-

[1] That was eight years after the Nature article on spin precession [2].

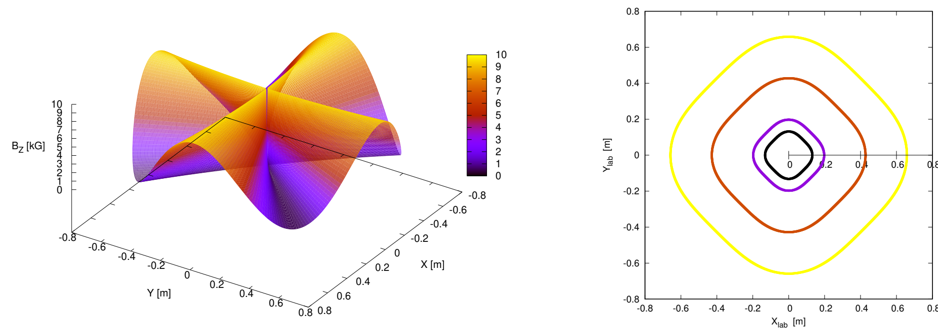

Fig. 4.1 Left: mid-plane magnetic field in a 4-periodic AVF cyclotron. Right: closed orbits around the cyclotron feature azimuthally varying curvature, greater on the hills, weaker in the field valleys

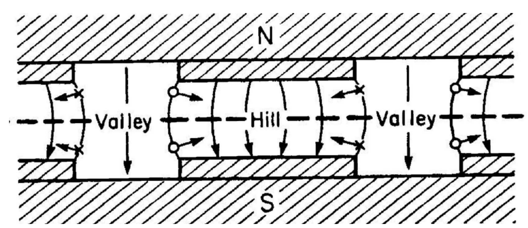

Fig. 4.2 Vertical azimuthal cross cut of an AVF cyclotron, showing the field hills (H) and valleys (V) [1]. Markers represent the radial component of the velocity vector, pointing alternately away from (cross) and toward the reader (circle); the resulting cross product with the magnetic field at the transition between the H and V regions is (positive charge is assumed) a force toward the median plane (arrows)

nism, as an AVF results in vertical focusing (Fig. 4.2), or equivalently in a correction of the vertical wave number, namely

$$\nu_y = \sqrt{-k + F^2} = \sqrt{-\beta^2\gamma^2 + F^2} \tag{4.1}$$

with F a parameter quantifying the field modulation (Eq. 4.8): strong enough field modulation results in $F > \beta\gamma$. Spiral pole geometry (Eq. 4.11, Fig. 4.9) came on the scene in 1954 [4], it allows increasing the axial focusing and thus higher energies. The first AVF cyclotron was operated in 1957, tens followed within the next decade, accelerating all sorts of ions, polarized beams, allowing variable energy [7], and application in a variety of domains as material science, radiobiology, production of beams of secondary particles. The concept of field sectors in the AVF cyclotron eventually led to the separated sector cyclotron in 1963: drifts between magnets allow room for higher efficiency extraction systems and thus higher beam current, for high-Q RF resonators resulting in greater turn separation, so facilitating the design of multiple stage high energy installations, and for beam monitoring instrumentation. Cyclotron energy and size subsequently increased, up to the present days GeV range. Cryogeny joined the scene in 1962, with the Michigan State University K500 superconducting coil cyclotron [6], allowing higher field and reduction of size. Radioisotope production and proton therapy applications have seen a quick increase in the number of AVF cyclotrons in the recent years.

Table 4.1 A comparison between an AVF and a separated sector cyclotron of same energy, 72 MeV (namely, former Injector 1 and present Injector 2 of PSI high power cyclotron, after Ref. [7, p. 126])

		AVF	separated sector
Injection energy	keV	14	870
Extraction energy	MeV	72	72
Magnet		single dipole	4 sectors
Weight	ton	470	4×180
Gap	mm	240 to 450	35
$\langle B \rangle$; B_{max}	T	1.6; 2	0.36; 1.1
RF system		180^o dees	2 resonators
Max accelerating voltage	kV	2×70	4×250
RF frequency	MHz	50	50
Normalized beam emittance, hor.; vert.	μm	2.4; 1.2	1.2; 1.2
Beam phase width	deg	16 - 40	12
Energy spread	%	0.3	0.2
Turn separation at extraction	mm	3	18

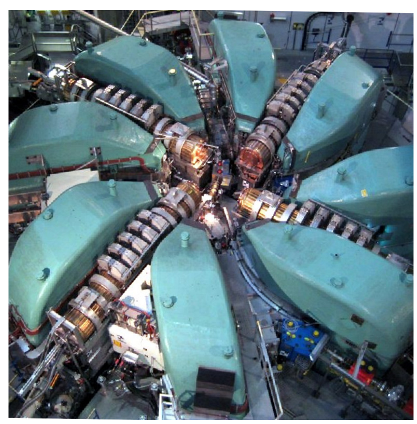

Fig. 4.3 PSI 590 MeV, 1.4 MW ring cyclotron, 15 m diameter. Proton acceleration takes ~180 turns. Beam extraction efficiency 99.99%. Delivers beams for secondary particle production including neutrons and muon beams [8]

To this day, thousands of cyclotrons have been built, tens are produced each year, applications include proton therapy, production of radio-isotopes, high power proton beams, secondary particle beams. Cryogeny and high fields further allow compactness (Fig. 4.4) [9] and higher rigidities (Fig. 4.5) [10]

Fig. 4.4 COMET at PSI. A 250 MeV, 500 nA, 4-sector isochronous AVF cyclotron, the spiral poles ensure vertical focusing. A 3 m diameter superconducting-coil provides the field. Delivers beams for proton therapy [9]

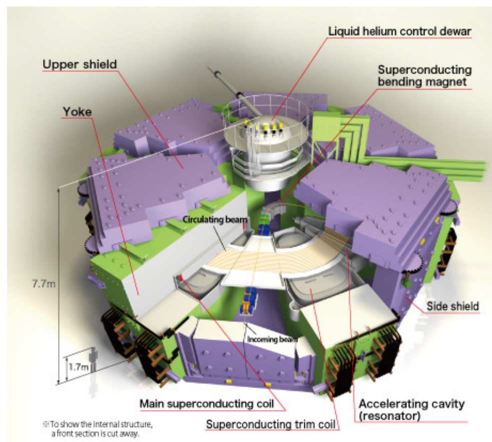

Fig. 4.5 RIKEN K1300, superconducting coil, separated-sector, ion cyclotron, 3.8 T field and 8 T m rigidity, 18.4 m in diameter, 8300 ton. Beam injection radius 3.56 m, extraction radius 5.36 m [11]

4.1 Theory, Basic Concepts

In the classical cyclotron, the relativistic increase of the mass slows down particles as energy increases, causing loss of synchronism, and the necessary negative field index for vertical focusing adds to that. Instead, constant $\omega_{\rm rev} = qB/\gamma m_0$, given $\rm R = \beta c/\omega_{rev}$, leads to

$$\rm k = \frac{R}{B}\frac{\partial B}{\partial R} = \frac{\beta}{\gamma}\frac{\partial \gamma}{\partial \beta} = \beta^2\gamma^2 \qquad (4.2)$$

Thus isochronism of revolution motion requires k to be positive and follow the energy increase: the weak focusing condition $-1 < \rm k < 0$ can not be satisfied, transverse periodic stability is lost.

The revolution period on the equilibrium orbit, momentum $\rm p = qBR$ and circumference C, is $\rm T_{rev} = C/\beta c = 2\pi\gamma m_0/qB$. Isochronism requires p-independent revolution period, $\rm dT_{rev}/dp = 0$. Differentiating the previous expression, this yields

$$B(R) = \frac{B_0}{\gamma_0}\gamma(R) \tag{4.3}$$

with B_0 and γ_0 some reference conditions,

This led H.A. Bethe and M.E. Rose to conclude [12] *"... it seems useless to build cyclotrons of larger proportions than the existing ones... an accelerating chamber of* 37 *cm radius will suffice to produce deuterons of* 11 *MeV energy which is the highest possible..."*. Frank Cole : "If you went to graduate school in the 1940s, this inequality $[-1 < k < 0]$ was the end of the discussion of accelerator theory."

Until...

4.1.1 Thomas Focusing

"*It is shown in detail below that a variation of magnetic field proportional to* $cos 4\theta$, [...] *admits a stable family of closed orbits that are approximately circles about the center of the cyclotron. Thus a variation of the magnetic field with angle,* [...] *and of order of magnitude v/c*; *together with nearly the radial increase of relative amount* $\frac{1}{2}v^2/c^2$ *of Bethe and Rose*; *gives stable orbits that are in resonance and not defocused."* [3]: this was the transition to the isochronous cyclotron in 1938, with the introduction by L.H. Thomas of the concept of polar variation of the axial field, the "AVF" (Azimuthally Varying Field) cyclotron (Fig. 4.6). Off mid-plane, the radial component of the velocity vector bends the trajectories toward the median plane (Fig. 4.2); this is sketched in the hard edge model in Fig. 4.7.

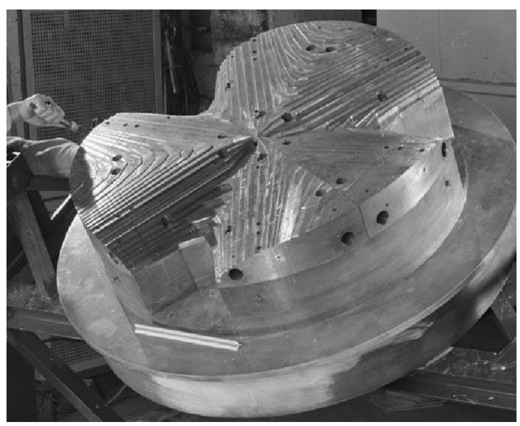

Fig. 4.6 Azimuthal pole shaping in an AVF cyclotron, an electron model, here [1]. The focusing pattern is FfFfFf, an alternation of strong (hill regions) and weak (valleys) radial focusing

AVF axial focusing is introduced in proper amount to compensate the axial defocusing effect resulting from k following $\beta^2\gamma^2$ (Eq. 4.2), which in turn ensures T_{rev}=constant. This is still today the technology of cyclotrons in the few tens of

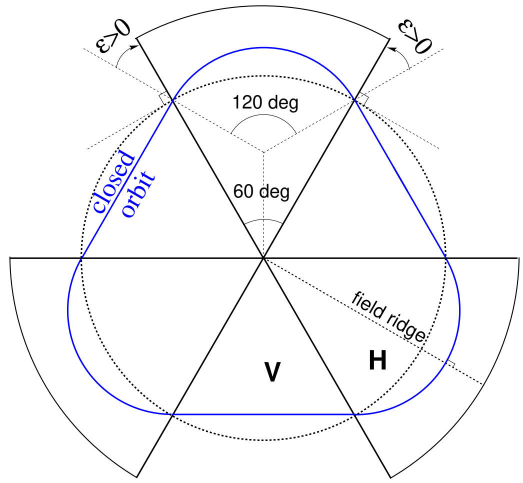

Fig. 4.7 Sketch of a 3-periodic, 60 deg radial sector AVF cyclotron, in a hard-edge model (zero field between the poles, azimuthally constant field across the poles). The closed orbit is at an $\varepsilon = 30^{\mathrm{o}}$ "wedge angle" from the sector edges. The wedge is closing, so introducing vertical focusing, and weakening the horizontal focusing. Note that the closed orbit is normal to the field ridge in the hill region, by symmetry

MeV range, for isotope production mostly, and up to 200 MeV and beyond for proton therapy application.

The single-magnet concept of the classical cyclotron remains, however the magnet pole is shaped to introduce a $2\pi/\mathrm{N}$-periodical field modulation (Figs. 4.4, 4.6). A convenient analytical approach consists in assuming a sinusoidal azimuthal dependence of the field, writing

$$\mathcal{F}(\theta) = 1 + \mathrm{f}\sin(\mathrm{N}\theta) \tag{4.4}$$

This modulation of the field results in a so-called "scalloping" of the orbit, around the reference circle (Fig. 4.7).

The necessary radial increase of the field for preserving the isochronism of the orbits in the relativistic regime (Eq. 4.3) may be obtained by introducing a radial dependence of the pole profile (Fig. 4.6). The mid-plane field can thus be expressed under the form

$$B(R,\theta) = B_0\,\mathcal{R}(R)\,\mathcal{F}(\theta) \tag{4.5}$$

The orbit curvature varies along the $\frac{2\pi}{N}$-periodic orbit. This requires distinguishing between the local focusing index

$$n = \frac{\rho(s)}{B(s)}\frac{dB}{d\rho} \tag{4.6}$$

and a geometrical index

$$k = \frac{R}{B}\frac{dB}{dR} \tag{4.7}$$

a global quantity which determines two others, namely the wave numbers of the transverse oscillatory particle motion (Eq. 4.10).

Edge Focusing

Edge focusing is a local effect of the entrance and exit ends of a dipole. In the AVF cyclotron the wedge angle is positive (Fig.4.8), first order horizontal defocusing results. First order vertical focusing results from the angle of the particle velocity vector to the azimuthal component of the field at magnet edge; a first order correction has to be added to account for the fringe field extent. More on edge focusing can be found in Section 18.4.3.

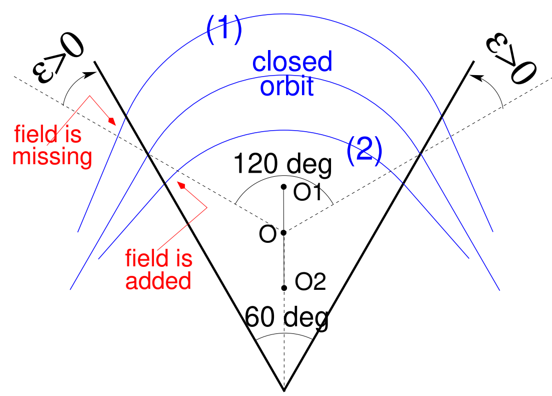

Fig. 4.8 A 120 deg bending of the closed orbit (curvature center at O) is ensured by a 60 deg sector dipole. This results in $\varepsilon = 30$ deg "wedge angles" at the entrance and exit face of the 60 deg sector dipole. The angle of the trajectories to the azimuthal field component results in vertical focusing of off mid-plane trajectories. The wedge angle causes a decrease in the horizontal focusing: trajectory (1) (curvature center at O1) is bent less due to missing field, trajectory (2) (curvature center at O2) is bent more due to added field

A "flutter" factor, F, can be introduced to quantify the focusing effect of the azimuthal modulation of the field. For a given orbit, of average radius R $= C/2\pi$ and local curvature ρ(s), it writes

$$\mathrm{F} = \left(\frac{<(\mathcal{F}-<\mathcal{F}>)^2>}{<\mathcal{F}>^2}\right)^{1/2} \xrightarrow{\text{hard edge}} \left(\frac{\mathrm{R}}{\rho}-1\right)^{1/2} \tag{4.8}$$

wherein $<*>=\oint(*)\,d\theta/2\pi$. R/ρ is the value reached in the limit where the field is null in the valleys, azimuthally constant in the hill regions (hard-edge sector field model). If the scalloping of the orbit is small, *i.e.*, $C/2\pi \approx \rho$, and accounting for the isochronism condition $k = \beta^2\gamma^2$ then

$$\nu_R \approx \sqrt{1+k} = \gamma, \qquad \nu_y \approx \sqrt{-k+F^2} \overset{\text{isochr.}}{=} \sqrt{-\beta^2\gamma^2+F^2} \tag{4.9}$$

$$\nu_R^2+\nu_y^2 = 1+F^2 \xrightarrow{\text{hard edge}} \frac{R}{\rho}$$

The flutter results in $-\mathrm{k} + \mathrm{F}^2 > 0$ (whereas $\mathrm{k} > 0$ as B increases with R to ensure isochronism) thus the vertical motion features periodic stability.

Note that in the hypothesis of sinusoidal azimuthal field modulation of Eq. 4.4, one has $F = f/\sqrt{(2)}$ and

$$\nu_\mathrm{y} \approx \sqrt{-\mathrm{k} + \mathrm{f}^2/2}, \qquad \nu_\mathrm{R}^2 + \nu_\mathrm{y}^2 = 1 + \mathrm{f}^2/2 \tag{4.10}$$

4.1.2 Spiral Sector

Spiral sector geometry was introduced in 1954 in the context of FFAG studies [4], and found application in cyclotrons (as seen in the COMET cyclotron, Fig. 4.4). Spiraling the edges results in stronger vertical focusing (Eq. 4.13) compared to a radial sector (Eq. 4.10), it also permits an increase of the wedge angle with momentum (*i.e.*, with the radius, Fig. 4.9), so maintaining proper compensation of the increase of $k(R)$. A convenient analytical approach consists in assuming an azimuthally sinusoidal modulation

$$\mathcal{F}(\mathrm{R}, \theta) = 1 + \mathrm{f} \sin\left[\mathrm{N}\left(\theta - \tan(\xi)\ln\frac{\mathrm{R}}{\mathrm{R}_0}\right)\right] \tag{4.11}$$

whereas the mid-plane field writes under the form

$$\mathrm{B}(\mathrm{R}, \theta) = \mathrm{B}_0\, \mathcal{R}(\mathrm{R})\, \mathcal{F}(\mathrm{R}, \theta) \tag{4.12}$$

The magnet edge geometry is given by (Fig. 4.9)

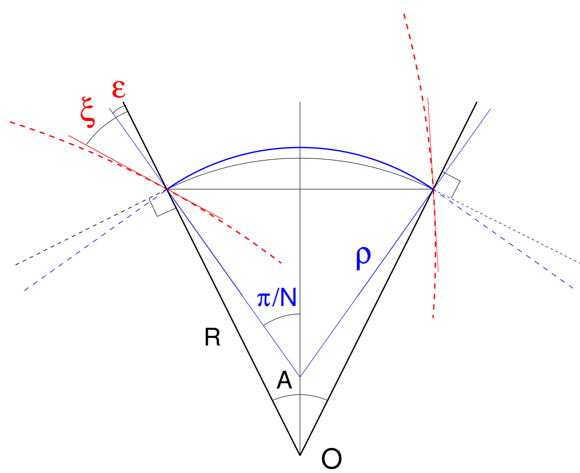

Fig. 4.9 Geometrical parameters of a $2\pi/N = A$ sector dipole of a N-sector cyclotron. 'O' is the center of the ring. The dashed lines figure the edges in the case of a spiral sector with spiral angle ξ at radius R (ξ increases with radius). A $p = qB\rho$ momentum closed orbit follows an arc with local curvature radius $\rho(\theta)$ (field varies along the arc). In the hard edge field model, an R-radius circle is a line of constant field inside the sector, null outside

$$r = r_0 \exp(\theta/\tan(\xi))$$

a logarithmic spiral centered at the center of the ring, with ξ the spiral angle, the angle that the tangent to the spiral edge does with the ring radius. This results in a larger contribution of the flutter term in the vertical wave number,

$$\nu_{\mathrm{y}} = \sqrt{-\mathrm{k} + \mathrm{F}^2(1 + 2\tan^2\xi)} \tag{4.13}$$

Since the field index k increases, to ensure isochronism (Eq. 4.2), the spiral angle has to follow, increase with radius, so to maintain $-k + F^2(1 + 2\tan^2\xi) > 0$. A limitation here is the maximum spiral angle achievable: $\xi \to 90$ deg means magnet edge going parallel to the closed orbit!

As an illustration, in TRIUMF cyclotron in the 500 MeV region, ξ increases to 72 deg (from null in the 100 MeV region) whereas $1 + 2\tan^2\xi$ increases to 20 (from 1 in the 100 MeV region) and compensates a low $F < 0.07$ (down from $F = 0.3$).

Most isochronous cyclotrons over a few tens of MeV use spiraled sectors [1], to benefit from the more efficient vertical focusing.

4.1.3 Separated Sector Cyclotron

The separated sector ring cyclotron came on the scene in the early 1960s. PSI 590 MeV ring is an example of a separated spiral sector lattice (Fig. 4.3). Its 70 MeV

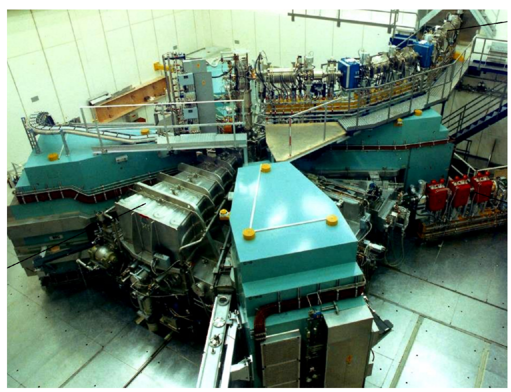

Fig. 4.10 PSI injector II, four separated radial sectors, 0.87 MeV injection energy, accelerates protons to 72 MeV in 100 turns. The drifts house 50.7 MHz RF and a flattop cavity. Injection is from the top, in the central region

injector is another example, a radial sector lattice (Fig. 4.10). The separated dipole structure is akin to the mid-1950s separated sector radial and spiral FFAGs (Chapter 10) (often considered part of the cyclotron family). The sector dipoles are separated by iron-free spaces - not necessarily field-free owing to fringe fields.

High energy cyclotrons in general use spiral sector optics, as it allows stronger vertical focusing resulting from the spiral angle. For instance, ξ reaches 72^o at 505 MeV in TRIUMF H^- 520 MeV cyclotron (from zero in the 100 MeV range); ξ reaches 35^o in PSI 500 MeV H^+ cyclotron.

The limit in energy of the separated sector cyclotron resides in the achievable field strength, magnet and overall cyclotron size, acceleration rate and achievable beam separation between the last two turns for extraction.

Fringe Field

In separated sector cyclotrons, the flutter factor (Eqs. 4.4, 4.11) which characterizes the azimuthal modulation of the field (Eqs. 4.5, 4.12) arises from the limited azimuthal extent of the dipoles and resulting fringe fields. A convenient model for the latter is (see Sec. 18.5)

$$F(d) = \frac{1}{1 + \exp P(d)} \tag{4.14}$$

$$P(d) = C_0 + C_1\left(\frac{d}{\lambda}\right) + C_2\left(\frac{d}{\lambda}\right)^2 + C_3\left(\frac{d}{\lambda}\right)^3 + C_4\left(\frac{d}{\lambda}\right)^4 + C_5\left(\frac{d}{\lambda}\right)^5$$

For the record, d is the distance to the magnet EFB, λ is a length which characterizes the extent of the fringe field (about the height of the dipole gap). The numerical values of $C_0 - C_5$ coefficients are determined so to match the fringe field shape (*e.g.*, constant in a simpler model, R-dependent in a fancier model accounting for R-dependence of the fringe field shape and extent).

4.1.4 Isochronism

In the hypothesis of isochronism, the revolution angular frequency satisfies

$$\omega_{\text{rev}} = \frac{c\beta(\gamma)}{R(\gamma)} = \text{constant}$$

An orbital radius $R_\infty = c/\omega_{\text{rev}}$ is reached asymptotically as $\beta = v/c = R/R_\infty \to 1$. In terms of the RF frequency and harmonic number,

$$R_\infty = h\frac{c}{\omega_{\text{rf}}} \tag{4.15}$$

Given $BR_\infty = \gamma m_0 c/q$ and using $\gamma = (1 - (R/R_\infty)^2)^{-1/2}$, the field on the orbit can be expressed in terms of R_∞, namely,

$$B(R) = \gamma B_0 = \frac{B_0}{\sqrt{1 - (R/R_\infty)^2}} \qquad \text{with } B_0 = \frac{m_0\omega_{\text{rev}}}{q} = \frac{m_0}{q}\frac{\omega_{\text{rf}}}{h} \tag{4.16}$$

and goes to infinity with $R \to R_\infty$.

For protons, , with $m_0 = 1.6726 \times 10^{-27}$ kg, $q = 1.6021 \times 10^{-27}$ C, $BR_\infty[T\,m] = \gamma m_0 c/q = 3.1\gamma$. A typical value for R_∞ can be obtained assuming for instance an upper $\gamma = 1.64$ (600 MeV) in a region of upper field value $B = 1.64$ T, yielding $R_\infty \approx 3.1$ m.

Radial field law

From Eq, 4.16 it results that the radial field form factor of Eqs. 4.5, 4.12 can be written

$$\mathcal{R}(R) = \left(1 - \left(\frac{R}{R_\infty}\right)^2\right)^{-1/2} \tag{4.17}$$

with $R_\infty = c/\omega_{\text{rev}}$. A possible approach consists in using the Taylor expansion of $\mathcal{R}(R)$ (within the limits of convergence of that series), namely

$$\mathcal{R}(R) = 1 + \frac{1}{2}\left(\frac{R}{R_\infty}\right)^2 + \frac{3}{8}\left(\frac{R}{R_\infty}\right)^4 + \frac{5}{16}\left(\frac{R}{R_\infty}\right)^6 + \ldots \tag{4.18}$$

The coefficients in this polynomial in R/R_∞ are the field index and its derivatives, they can be a starting point for further refinement of the isochronism, including for instance side effects of the azimuthal field form factor $\mathcal{F}(R, \theta)$ (Eqs. 4.4, 4.11).

Wave numbers

It follows from Thomas focusing that the radial field index in the AVF can be set positive and increase with radius to satisfy $k = \frac{R}{B}\frac{\partial B}{\partial R} = \beta^2\gamma^2$ (Eq. 4.2). Limiting any phase slip to substantially less $\pm\pi/2$ requires a tolerance below 10^{-5} on field error. Adjusting $k(R)$ to ensure such accuracy is a long process and includes pole machining, shimming, and other correction coil strategies. The isochronism constraint determines the wave numbers, namely

$$\nu_\text{R} = \gamma \quad \text{and} \quad \nu_\text{y} = \sqrt{-\beta^2\gamma^2 + \text{F}^2(1 + 2\tan^2\xi)} \tag{4.19}$$

wherein flutter F and spiral angle ξ are R-dependent quantities.

4.1.5 Fast Acceleration

Fixed field and fixed RF frequency in a cyclotron allow fast acceleration, a limitation is in the amount of voltage which can be installed. In high power cyclotrons, the voltage per turn reaches megavolts, about 4 MV for instance at the PSI 590 MeV ring cyclotron, where bunches are accelerated from 72 MeV to 590 MeV in less than 200 turns.

Fast acceleration results in fast crossing of harmful betatron resonances. For instance the "Walkinshaw resonance" $\nu_R = 2\nu_y$, which may lie across the beam path in the wave number diagram, as $\nu_R \approx \gamma$ whereas the vertical wave number takes its value in the $\nu_y \approx 1^- \sim 1.5$ region. This resonance causes the horizontal motion to couple to the vertical motion, resulting in increased vertical beam size and subsequently particle losses in the the vacuum chamber walls.

Fast acceleration improves extraction efficiency, as the turn separation dR/dn is proportional to the energy gain per turn (Sec. 4.1.6).

4.1.6 Cyclotron Extraction

From $R = p/qB$ and assuming constant field (which may be legitimate in the presence of a very small field index), one draws

$$\frac{dR}{R} = \frac{dp}{p} = \frac{E\,dE}{E^2 - M^2} \tag{4.20}$$

The minimum radial distance between the last two turns, where the extraction septum is located, is imposed by beam loss tolerances. Space charge in particular matters, as it increases the energy spread, and thus the radial extent of a bunch. In the relativistic cyclotron the separation between two consecutive turns satisfies

$$\Delta R \approx \frac{\gamma}{\gamma + 1} \frac{\Delta E}{E} \frac{R}{\nu_R^2} \tag{4.21}$$

with ΔE the effective acceleration rate per turn. In particular, the latter can be shown to constrain the current limit, namely [13]

$$\text{current limit } \propto (\Delta E)^3$$

Equation 4.15 indicates that a greater RF harmonic allows greater extraction radius, benefits extraction efficiency. It results from Eq. 4.21 that a large ring has similar effect, whereas on the contrary size is a limitation to intensity in small cyclotrons.

In low energy cyclotrons (γ close to 1), extraction efficiency may also be increased by moving the wave number $\nu_R \approx \gamma$ close to $\nu_R = 1$ resonance.

4.1.7 Resonant Spin Motion

Spin precession during the cyclic motion of a particle in the field of a cyclotron dipole satisfies (Sec. 18.6.1)

$$\frac{d\mathbf{S}}{dt} = \frac{q}{m}\,\mathbf{S}\times\boldsymbol{\omega}_{\rm sp} \tag{4.22}$$

with $\omega_{\rm sp}$ the precession vector. By analogy with betatron wave numbers, a precession frequency can been introduced, $\nu_{\rm sp} = G\gamma$, the number of spin precessions per turn.

If an ion travels in the bend plane (the median plane of the cyclotron dipole), it only experiences a magnetic field normal to its velocity, namely, $\mathbf{B}|_{\rm y=0} \equiv \mathbf{B}_y$, thus its spin precession vector

$$\boldsymbol{\omega}_{\rm sp} = \frac{q}{m_0\gamma}\,\left[(1+G)\mathbf{B}_{\parallel} + (1+G\gamma)\mathbf{B}_{\perp}\right]$$

reduces to $\boldsymbol{\omega}_{\rm sp} = \dfrac{q}{m_0\gamma}\,(1+G\gamma)\mathbf{B}_{\perp}$, the spin precesses around $\mathbf{B}_{\perp} \equiv \mathbf{B}_y$, the angle $(\mathbf{S}, \mathbf{B}_y)$ remains unchanged during particle motion.

In the AVF cyclotron, due to the azimuthal field modulation (Eq. 4.4) and to the radial index (Eq. 4.2), the azimuthal and radial field components B_θ and B_R are non-zero out of the median plane (Maxwell equations). Thus the local spin precession axis is not vertical, and the precession vector that the ion experiences changes as it oscillates vertically about the median plane. Resonance between spin precession (characterized by spin tune $\nu_{\rm sp} = G\gamma$) and vertical particle oscillation motion (wave number ν_y) occurs if the two motions feature coinciding frequencies. This condition can be written under the form

$$\nu_{\rm sp} \pm \nu_y = \text{integer} \tag{4.23}$$

Near the resonance, at fixed energy (constant spin tune $\nu_{\rm sp} = G\gamma$), the torque that the magnetic field exerts periodically causes the spins to tilt away from the vertical, the spin precession axis is at an angle to the vertical. Exactly on the resonance ($\nu_{\rm sp} \pm \nu_y$ = integer) the spin precession axis lies in the median plane. As a consequence, when a particle crosses the resonant condition (Eq. 4.23) during acceleration, its spin precesses away from the initial precession direction. Assuming an isolated resonance, the initial ($S_{\rm y,i}$) and final ($S_{\rm y,i}$) values of the vertical spin components, respectively far upstream and far downsteam of the resonance, satisfy the Froissart-Stora rule [14]

$$\frac{S_{\rm y,f}}{S_{\rm y,i}} = 2e^{-\frac{\pi}{2}\frac{|\epsilon_R|^2}{\dot{\Delta}}} - 1 \tag{4.24}$$

The magnitude of the tilt (*i.e.*, the amount that the $(\mathbf{S}, \mathbf{B}_y)$ angle is changed under the effect of the resonance crossing, from $(\mathbf{S}_{\rm y,i}, \mathbf{B}_y)$ to $(\mathbf{S}_{\rm y,f}, \mathbf{B}_y)$) depends on the strength of the resonance, $|\epsilon_R|$, and on the crossing speed, *i.e.*, the rate of change of the distance to the resonance $\Delta = \nu_{\mathrm{sp}} \pm \nu_y - \text{integer}$,

$$\dot{\Delta} = \frac{d\nu_{\mathrm{sp}}}{dt} \pm \frac{d\nu_y}{dt} \tag{4.25}$$

In particular, if the resonance is crossed very slowly, the spin will follow the motion of the precession axis from vertical before the resonance to vertical after the resonance. If the crossing is very fast, spins maintain their initial angle to the vertical.

4.2 Exercises

Preliminaries

- Zgoubi users' guide at hand, when setting up the input data files to work out the exercises, is a must-have. PART B of the guide in particular, details the formatting of the input data lists following keywords (a few keywords only, for instance FAISCEAU, MARKER, YMY, do not require additional data), and gives the units to be used.
- About keywords: by "keyword" it is meant, the name of the optical elements, or I/O procedures, or commnads, as they appear in simultaion input data file. Keywords are most of the time referred to without any additional explanation: it is understood that the users' guide is at hand, and details regarding the use and functionning to be sought there: in PART A of the guide, as to what a particular keyword does and how it does it; in PART B as to the formatting of the data list under a particular keyword. The users' guide INDEX is a convenient tool to navigate through the keywords.
  - The notation KEYWORDS[ARGUMENT1, ARGUMENT2, ...]: it uses the nomenclature found in the Users' Guide, Part B. Consider a couple of examples:
    - OBJET[KOBJ=1] stands for keyword OBJET, and the value of KOBJ=1 retained here;
    - OPTIONS[CONSTY=ON] stands for keyword OPTIONS, and the option retained here, CONSTY, switched ON.
  - The keyword INCLUDE is used in many simulation input data files. The reason is mostly to reduce the length of these files. It may always be replaced by the sequence theat it INCLUDEs.
- Coordinate Systems: two sets of coordinate notations are used in the exercises,

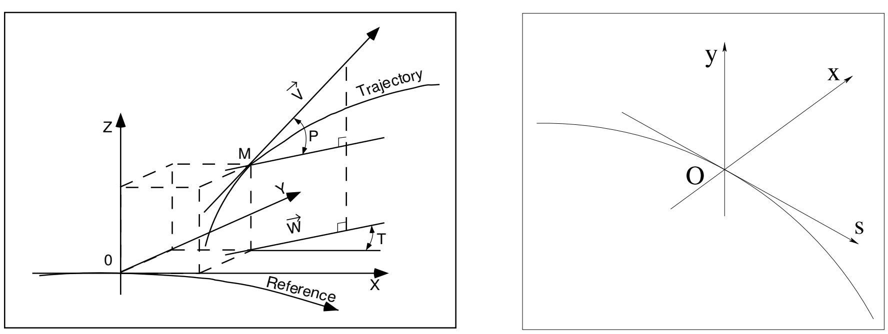

Fig. 4.11 Zgoubi Cartesian frame (O;X,Y,Z), and moving frame (O;s,x,y)

- on the one hand (and, in the Solutions Section mostly), zgoubi's (Y,T,Z,P,X,D) coordinates in the optical element reference frame (O;X,Y,Z), the very frame in which the optical element field $\mathbf{E}(X,Y,Z)$ and/or $\mathbf{B}(X,Y,Z)$ is defined (the origin for X depends on the optical element). Particle coordinates in this frame can be
  · either Cartesian, in which case X, Y (angle T) and Z (angle P) denote respectively the longitudinal, transverse horizontal and vertical coordinates,
  · or cylindrical, in which case, given m the projection of particle position M in the Z=0 plane, Y denotes the radius: $Y = |\mathbf{Om}|$, whereas X denotes the **OX**-**Om** angle (and, yes, the nature of the variables named X and Y in the source code does change);

  Note: the sixth zgoubi's coordinate above is

$$D = \frac{\text{particle rigidity}}{BORO}$$

  with BORO a reference rigidity, the very first numerical datum to appear in any zgoubi sequence, as part of the definition of initial particle coordinates by OBJET or MCOBJET. BORO may sometimes be denoted $B\rho_{\text{ref}}$, depending upon the context. Note that D-1 identifies with the above $\delta p/p$.
- on the other hand (and, in the exercise assignements mostly), the conventional (x,x',y,y',δl,$\delta p/p$) coordinates in the moving frame (O;s,x,y) or close variants.

Comments are introduced wherever deemed necessary (hopefully, often enough) in an effort to lift potential ambiguities regarding coordinate notations.

4.1 Modeling Thomas AVF Cyclotron

In this exercise a field map model of Thomas cyclotron is built (Fig. 4.1) and used to derive parameters of this 4-period AVF cyclotron. The field map is 2-dimensional, it describes the magnetic field in the median plane (the symmetry plane of the dipole magnet), in a polar coordinate system. TOSCA is used to handle and raytrace through that map [15].

A 2-dimensional m(R, θ) polar meshing of the median plane is used (as in Fig. 3.18, page 36). The median plane field map provides $B_Z(R,\theta)$ values of the field component normal to the (X,Y) plane, at the nodes of the mesh. Computation of the field along (R,θ) particle trajectories in the (O;X,Y,Z) frame is performed from the field map data, using interpolation techniques [15].

(a) Construct a 360^o 2-dimensional map of the median plane field $B_Z(R,\theta)$, simulating the field in the 4-period Thomas cyclotron of Fig. 4.1 and following (Eq. 4.4)

$$B_Z(R,\theta) = B_0[\,1 + f\,\sin(4(\theta-\theta_i))\,]$$

with θ_i some arbitrary origin of the azimuthal angle, to be determined (hint: depending on θ_i value, the closed orbit may be at an angle to the polar radius, as seen in Fig. 4.1; in that case TOSCA would require non-zero in and out positioning angles TE and TS, to be determined and stated using KPOS option [15]; instead, a proper choice of θ_i value allows TE=TS=0). Assume an average axial field $B_0 = 0.5$ T, $B_Z > 0$ and $0 < f < 1$ modulation. Use a uniform mesh in a polar coordinate system (R, θ) as sketched in Fig. 3.18, covering R=1 to 100 cm. Take a radial increment of the mesh $\Delta R = 0.5$ cm, azimuthal increment $\Delta\theta = 0.5$ cm/RM, with RM a reference radius as required in this process, say $RM = 50$ cm.

The appropriate 6-column formatting of the field map data for TOSCA to read them is the following:

$$\mathrm{R}\cos\theta,\ \mathrm{Z},\ \mathrm{R}\sin\theta,\ \mathrm{BY},\ \mathrm{BZ},\ \mathrm{BX}$$

with θ varying first, R varying second in that list. Z is the vertical direction (normal to the map mesh), so Z ≡ 0 in this 2-dimensional mesh.

Plot $B_Z(R, \theta)$ over the extent of the field map.

(b) Raytrace a few concentric closed trajectories centered on the center of the dipole, ranging in $10 \le R \le 80$ cm. Plot these concentric trajectories in the $(O; X, Y)$ laboratory frame. Initial coordinates can be defined using OBJET, particle coordinates along trajectories during the stepwise raytracing can be logged in zgoubi.plt by setting IL=2 under TOSCA.

(c) Check the effect of the integration step size on the accuracy of the trajectory and time-of-flight computation, by considering some Δs values in [0.1,10] cm, and energies in a range from 200 keV to a few tens of MeV (assume proton).

(d) Produce a graph of the R-dependence of wave numbers.

(e) Calculate the numerical value of the axial wave number, ν_y, from the flutter (Eq. 4.8). Compare with the numerical values: some discrepancy may be found: repeat (d) for f=0.1, 0.2, 0.3, 0.6, check the evolution of this discrepancy, find its origin.

4.2 Isochronism

(a) Demonstrate equation 4.2.

(b) Demonstrate equation 4.3.

(c) Devise numerical simulations proper to illustrate these relationships.

4.3 Designing an Isochronous AVF Cyclotron

(a) Introduce an R-dependent field index k(R) in the AVF cyclotron designed in exercise 4.1, proper to ensure R-independent revolution period, in three different cases of modulation: f=0 (no modulation), f=0.2 and f=0.9.

Check this property by computing the revolution period T_{rev} as a function of kinetic energy E_k, or radius R. On a common graph, display both T_{rev} and dT_{rev}/T_{rev} as a function of radius, including for comparison a fourth case: B=constant=5 kG.

(b) Plot the energy dependence of wave numbers.

4.4 Acceleration in an AVF Cyclotron

Produce an acceleration cycle of a single proton, from 0.2 to 100 MeV, in the AVF cyclotron designed in exercise 4.3. Assume proper modulation (coefficient f) for vertical focusing all the way to 300 Mev about. Assume a double-dee design, and 400 keV gap voltage, peak, use CAVITE[IOPT=7] for acceleration to account for RF phase.

4.5 Thomas-BMT Spin Precession in Thomas Cyclotron

This exercise uses the field maps and input data file of exercise 4.4. Dependence of energy boost on RF phase is removed by using CAVITE[IOPT=3] [15].

(a) Find the $G\gamma$ value for which the resonant condition (Eq. 4.23) is satisfied.

(b) Consider a helion particle with non-zero vertical motion, so that it experiences non-vertical magnetic field as it cycles around. Track its spin through the resonance, take initial spin vertical $\mathbf{S} \equiv \mathbf{S}_Z$. Plot S_Z as a function of $G\gamma$ and energy.

Calculate the crossing speed (Eq. 4.25).

(c) Simulate a series of spin tilts in the range $-1 < S_{\mathrm{y,f}}/S_{\mathrm{y,i}} < 1$, by varying the vertical motion amplitude, plot the ration $S_{\mathrm{y,f}}/S_{\mathrm{y,i}}$ of the final to initial value of the vertical spin component, as a function of the initial vertical coordinate of the particle.

(d) From a match of this $S_{\mathrm{y,f}}/S_{\mathrm{y,i}}$ series with Eq. 4.24, show that the resonance strength changes in proportion to the square root of the vertical motion invariant.

Produce a plot of the series of resonance crossing $\mathrm{S_Z}$(turn), for this series of Z_0 values.

(e) Repeat (c) by changing the resonance crossing speed instead (leaving Z_0 unchanged).

Show that this $S_{\mathrm{y,f}}/S_{\mathrm{y,i}}$ series can be matched with the expression of Eq. 4.24.

4.6 Edge Focusing, Flutter

In this exercise DIPOLES is used to simulate a 30 deg sector dipole of a 90 deg-periodic cyclotron, and reproduce the principle geometry of the isochronous AVF cyclotron of exercise 4.3 (PSI 4-sector 72 MeV injector II, Fig. 4.10, is an example of such 4-cell configuration with short dipoles). DIPOLES is chosen rather than DIPOLE as it allows radial field indices up to high order [15, Eq. 6.3.19], as needed to devise proper radial field profile, whereas DIPOLE does not go beyond a $\partial^3 B_Z/\partial R^3$ index [15, Eq. 6.3.17].

Take fringe fields into account (Eq. 4.15), with

- $\lambda = 7$ cm the fringe extent (changing λ changes the flutter, Eq. 4.8),

- $C_0 = 0.1455$, $C_1 = 2.2670$, $C_2 = -0.6395$, $C_3 = 01.1558$ and $C = 0$, for a realistic fringe field model.

(a) Assume $k = 0$, here. Produce a model of the 4-period AVF, accounting for a field extent λ as allowed by DIPOLE.

Plot closed orbits across a period for a few different particle rigidities - FIT can be used to find the closed orbits. Plot the field along these orbits.

(b) Proper R-dependence of the mid-plane magnetic field is now introduced, to ensure revolution period closest to energy independent. In that aim, DIPOLES field indices b_i are used.

Assume a peak field value $\hat{B} = 1.1$ T in the dipoles, at radius r=3.5 m. Find the average orbit radius R, and average field B (such that $BR = p/q$), at an energy of 72 MeV.

Determine a series of index values, $b_{i=1,n}$, in the model [15, Eq. 6.3.19]

$$B_Z(R,\theta) = B_0\,\mathcal{F}(R,\theta)\left(1 + b_1\frac{R-RM}{RM} + b_2\left(\frac{R-RM}{RM}\right)^2 + \dots\right) \tag{4.26}$$

proper to bring the revolution period closest to being R-independent, in the energy range 0.9 to 72 MeV (hint: use a limited Taylor development of Eq. 4.17 and identify with the R-dependent factor in Eq. 4.26).

(c) Play with the value of λ, concurrently to maintaining isochronism with appropriate transverse field index values. Check the evolution of horizontal and vertical focusing - OBJET[KOBJ=5] and MATRIX can be used to get the wave numbers.

Check the following, from raytracing trials:

(i) the effect of λ on horizontal focusing is weak (how does it contribute in the matrix formalism?),

(ii) greater (smaller) λ results in smaller (greater) flutter and weaker (stronger) vertical focusing. Note: the integration step size in `DIPOLE` has to be made consistent with the value of λ, in order to ensure that the numerical integration is converged.

(d) For some reasonable value of λ (normally, about the height of a magnet gap, say, a few centimeters), compute $\mathrm{F}^2 = \left\langle \left(\frac{\mathrm{B}(\theta)-<\mathrm{B}>}{<\mathrm{B}>}\right)^2 \right\rangle$, check $\nu_y = -\beta^2\gamma^2 + \mathrm{F}^2$ (Eq. 4.19). MATRIX can be used to compute ν_y, or otherwise Fourier analysis, however not as straight forward as it requires multiturn raytracing.

(e) Check the rule $F^2 \overset{\text{hard edge}}{\longrightarrow} \frac{R}{\rho} - 1$ (Eq. 4.8), from the field $B(\theta)$ delivered by DIPOLES. Give a theoretical demonstration of that rule.

4.7 PSI Ring Cyclotron, Using its Measured Field Map

PSI field map, named POLARMES_PSI_drift.H, can be found at

https://sourceforge.net/p/zgoubi/code/HEAD/tree/trunk/exemples/KEYWORDS/POLARMES/

POLARMES_PSI_drift.H is an ascii file, it contains the mid-plane field at the nodes of a two-dimensional cylindrical mesh. The mesh is 136×140 nodes, respectively azimuthally $\times$ radially.

(a) Explain why POLARMES is used rather than TOSCA[MOD=25] [15].

Set up a simulation data file to find a few closed orbits over PSI cyclotron energy range, 72 to 590 MeV. Hint: FIT can be used to find the periodic orbit coordinates. Assume a single particle defined in OBJET, REBELOTE can thus be used, following FIT, to repeat that sequence for a series of values of the relative rigidity of that particle. Use IL=2 under POLARMES to have step-by-step particle data logged in zgoubi.plt.

Plot these periodic orbits in a laboratory frame.

Plot the vertical component of the magnetic field along these closed orbits.

(b) Plot beam envelopes at 72 MeV, 590 MeV, and some intermediate energies.

(c) Do a dense orbit scan: 200 orbits over 72 – 590 MeV. Get from this scan a plot of the revolution time as a function of radius.

(d) Plot the beam path in the wave number diagram (consider paraxial wave numbers).

(e) Simulate a complete acceleration cycle, from 72 to 590 MeV, for a 200-particle 6D bunch, with initial transverse emittances 5πmm mrad, initial length 2 cm and *rms* momentum spread 10^{-3}, Gaussian. Assume 4 MV per turn, accelerating gaps located in four drift spaces as in Fig. 4.3.

(f) Repeat (e) with a initially 100% vertically polarized bunch. Check the transmission of the polarization (final polarization over initial polarization).

4.8 A Model of PSI Ring Cyclotron Using CYCLOTRON

The simulation input data file in Tab. 4.2 is based on the use of CYCLOTRON, to simulate a period of the eight-sector PSI ring cyclotron.

This file is the starting point of the present exercise.

(a) With zgoubi users' guide at hand, explain the signification of the data in that simulation input data file.

(b) Compute and plot the radius dependence of the revolution period. Comment on the isochronism.

(c) The field indices are aimed at realizing the isochronism (equal revolution period at all energies). Four are involved in (a) and (b), B1 to B4, they have been drawn from the PSI cyclotron cell field map data (exercise 4.7). Question (b) proves this small set of indices to result in poor isochronism.

Add higher order indices, until a sufficient number is found that FIT is able to reach a final isochronism improved by more than an order of magnitude.

Table 4.2 Simulation input data file: a period of an eight-sector cyclotron. The data file is set up for a scan of the periodic orbits, from radius R=204.1171097 cm to R=383.7131468 cm, in 15 steps

```
PSI CYCLOTRON

'OBJET'
1249.382414
2
1 1
204.1171097  8.915858372  0.  0.  0.  1.    'o'
1
'PARTICUL'
PROTON

'CYCLOTRON'
2
1   45.0  276.  1.0
0. 0. 0.99212277 51.4590015 0.5 800. -0.476376328 2.27602517e-03 -4.8195589e-06 3.94715806e-09
18.3000E+00  1.  28. -2.0
8 1.1024358 3.1291507 -3.14287154 3.0858059 -1.43545 0.24047436 0. 0. 0.
11.0  3.5 35.E-3  0.E-4 3.E-8 1. 1. 1.
18.3000E+00  1.  28. -2.0
8 0.70490173 4.1601305 -4.3309575 3.540416 -1.3472703 0.18261076 0. 0. 0.
-8.5  2.  12.E-3   75.E-6   0.E-6     1.  1.  1.
0. -1
0  0.  0.  0.  0.  0.  0.  0.
0.  0.  0.   0.  0.  0.
2  10.
0.4
2 0.  0. 0.  0.

'FIT2'
2
1 31 0 [-300.,100]
1 35 0 [.1,3.]
2
3.1 1 2 #End 0. 1. 0
3.1 1 3 #End 0. 1. 0
'FAISCEAU'

'FAISTORE'
orbits.fai
1

'REBELOTE'
14 0.2  0 1
1
OBJET 30 221.065356:383.7131468

'SYSTEM'
1
gnuplot <./gnuplot_orbits.gnu
'END'
```

References

1. Craddock, M.K.: AG focusing in the Thomas cyclotron of 1938, Proceedings of PAC09, Vancouver, BC, Canada, FR5REP1. http://accelconf.web.cern.ch/PAC2009/papers/fr5rep113.pdf
2. Thomas, L.H.: Motion of the spinning electron. Nature. 117 (2945): 514 (1926)
3. Thomas, L.H.: The Paths of Ions in the Cyclotron. Phys. Rev. 54, 580, (1938)
4. Symon, K.R., et al.: Fixed-Field Alternating-Gradient Particle Accelerators. Phys. Rev. 103, 1837 (1956)
5. Stammbach, T.: Introduction to Cyclotrons. CERN accelerator school, cyclotrons, linacs and their applications, IBM International Education Centre, La Hulpe, Belgium, 28 April-5 May 1994
6. Miller, P.S., et al.: The Magnetic Field of the K500 Cyclotron at MSU Including Trim Coils and Extraction Channels. Procs. 9th Int. Conf. on Cyclotrons and their Applications, September 1981, Caen, France. http://accelconf.web.cern.ch/c81/papers/ep-05.pdf
7. Stammbach, T.: Introduction to Cyclotrons. CERN accelerator school, cyclotrons, linacs and their applications, IBM International Education Centre, La Hulpe, Belgium, 28 April-5 May 1994
8. Seidel, M.: Production of a 1.3 Megawatt Proton Beam at PSI. Proceedings of IPACâĂŹ10, Kyoto, Japan, TUYRA03. http://accelconf.web.cern.ch/IPAC10/talks/tuyra03_talk.pdf
9. J.M. Schippers, J.M.: The Superconducting Cyclotron and Beam Lines of PSIâĂŹs New Proton Therapy Facility “PROSCAN”. 17th International Conference on Cyclotrons and their Applications: Tokyo, Japan; 18-22 October 2004. http://accelconf.web.cern.ch/c04/data/CYC2004_papers/20B2.pdf
10. http://accelconf.web.cern.ch/c07/OTHERS/Cyclotron%20List%202007%20-Full.pdf
11. Kawaguchi, T., et al., Design of the sector magnets for the RIKEN superconducting ring cyclotron, Proceedings of the 15th International Conference on Cyclotrons and their Applications, Caen, France. http://www.nishina.riken.jp/facility/SRC_e.html
12. Bethe, H.A. and Rose, M.E., Phys. Rev. 54, 588 (1938)
13. Joho, W.: The Cyclotron Facilities at PSI. Seminar slides, PSI, 2013 (unpublished)
14. Froissart, M., Stora, R.: Depolarisation d’un faisceau de protons polarises dans un synchrotron. Nuclear Instruments and Methods. 7 (3): 297âĂŞ305 (June 1960)
15. Méot, F.: Zgoubi Users’ Guide. https://www.osti.gov/biblio/1062013-zgoubi-users-guide Sourceforge latest version: https://sourceforge.net/p/zgoubi/code/HEAD/tree/trunk/guide/Zgoubi.pdf